

Published in final edited form as:

J Pediatr Surg. 2009 June ; 44(6): 1120–1126. doi:10.1016/j.jpedsurg.2009.02.038.

Sternal Repair with Bone Grafts Engineered from Amniotic Mesenchymal Stem Cells

Shaun A. Steigman, MD¹, Azra Ahmed, BS¹, Rabie M. Shanti, BS¹, Rocky S. Tuan, PhD², Clarissa Valim, MD, PhD¹, and Dario O. Fauza, MD, FAAP¹

¹Department of Surgery, Children's Hospital Boston and Harvard Medical School, Boston, Massachusetts 02115

²Cartilage Biology and Orthopaedics Branch, NIAMS, National Institutes of Health, Department of Health and Human Services, Bethesda, MD 20892

Abstract

Background—We aimed at determining whether osseous grafts engineered from amniotic mesenchymal stem cells (aMSCs) could be employed in postnatal sternal repair.

Methods—Leporine aMSCs were isolated, identified, transfected with green fluorescent protein (GFP), expanded, and seeded onto biodegradable electrospun nanofibrous scaffolds (n=6). Constructs were dynamically maintained in an osteogenic medium and equally divided into two groups with respect to time *in vitro*, namely 14.6 or 33.9 weeks. They were then used to repair full thickness sternal defects spanning 2–3 intercostal spaces in allogeneic kits (n=6). Grafts were submitted to multiple analyses 2 months thereafter.

Results—Chest roentgenograms showed defect closure in all animals, confirmed at necropsy. Graft density as assessed by micro-CT scans increased significantly *in vivo*, yet there were no differences in mineralization by extracellular calcium measurements pre- and post-implantation. There was a borderline increase in alkaline phosphatase activity *in vivo*, suggesting ongoing graft remodeling. Histologically, implants contained GFP-positive cells and few mononuclear infiltrates. There were no differences between the two construct groups in any comparison.

Conclusions—Engineered osseous grafts derived from amniotic mesenchymal stem cells may become a viable alternative for sternal repair. The amniotic fluid can be a practical cell source for engineered chest wall reconstruction.

Index Words

tissue engineering; amniotic mesenchymal stem cells; mesenchymal stem cells; amniotic fluid; chest wall anomalies; nanofibers; fetus; sternum; congenital anomalies

Major congenital chest wall defects pose significant morbidity and mortality to infants [1]. Repair is often hindered by lack of sufficient tissue available for surgical reconstruction, particularly in the neonatal period [2, 3]. Operative management of these conditions often involves at least two-stages: early soft-tissue coverage of the mediastinum and/or pleural cavity, followed by some form of a more definitive chest wall reconstruction up to a few

Address correspondence to: Dario O. Fauza, M.D., Children's Hospital Boston, 300 Longwood Ave., Fegan 3, Boston, MA 02115, Phone: (617) 919-2966, Fax: (617) 730-0910, dario.fauza@childrens.harvard.edu.

Presented at the 60th Annual Meeting of the Section on Surgery, American Academy of Pediatrics, Boston, MA, October 10–12, 2008.

years thereafter [4, 5]. Overall, these procedures have proven challenging at best and survival rates for many of these conditions remain quite low [2].

As is customary when an optimal procedure for the treatment of a given disease has yet to be described, various methods of chest wall reconstruction have been reported in the setting of congenital defects, including autologous bone and cartilage grafts, musculocutaneous flaps, as well as coverage with prosthetic materials [2]. Almost invariably, these procedures have been associated with significant complications, such as infection, growth restriction, residual thoracic deformity, and donor site morbidity. We have previously shown that three-dimensional (3D) osseous grafts can be engineered from an abundant and easily accessible prenatal cell source, namely naturally occurring amniotic mesenchymal stem cells (aMSCs) [6]. In this study, we wished to start exploring, in an animal model, whether an aMSC-based fetal tissue engineering solution could become a viable alternative for the treatment of chest wall defects already in the neonatal period.

1. Materials and Methods

This study was approved by the Institutional Animal Care and Use Committee of Children's Hospital Boston under protocol number A05-12-104.

1.1. Cell Isolation, Expansion, and Labeling

Time-dated pregnant New Zealand does at 23–24 days gestation (term = 32 days; n=5) were anesthetized with 1–3% isoflurane (Baxter Healthcare, Deerfield IL) and received 20mg/kg of cefazolin (Orchid Healthcare, India) intravenously prior to surgical manipulation. A midline laparotomy was performed, followed by hysterotomies on the two distal-most amniotic cavities of the uterine horns. Amniotic fluid samples (0.6–0.9 mL; n=10) were then obtained under hemostatic conditions. The myometrium and gestational membranes were closed in a single layer with simple running 4-0 monofilament polypropylene sutures (Prolene, Ethicon, Somerville NJ). The abdominal wall was closed in layers and animals were allowed to recover.

Mesenchymal stem populations were isolated from the amniotic samples by a combination of natural selection with culture media and mechanical separation, as previously described by our group for ovine and human samples [7–9]. Briefly, samples were processed within less than 4 hours of procurement. The amniotic fluid specimen was centrifuged at 400 *g* for 15 minutes. The pellet was resuspended in 3 mL of growth medium consisting of high-glucose Dulbecco's Modified Eagle Medium with L-glutamine (Fisher Scientific, Fairlawn, NJ), 20% fetal bovine serum (FBS, Invitrogen, Carlsbad, CA), 5 ng/mL basic fibroblast growth factor (Promega, Madison, WI), 10,000 U/mL penicillin G sodium (Fisher), and 10 mg/mL streptomycin (Fisher). Cells were cultured in 6-well plates pre-coated with collagen type-I (BD Biosciences, San Jose, CA) and placed in a 5% CO₂ incubator at 37°C. After 2 days, nonadherent cells were discarded and 3 mL of fresh media was added to each well. Medium was subsequently changed twice weekly. Cells were inspected daily under an inverted microscope (Axiovert 40; Carl Zeiss, Jenna, Germany). Wells containing predominantly morphologically distinct, rapidly dividing cells were passaged using 0.05% trypsin and 0.53 mM EDTA (Invitrogen). After two passages, the FBS in the culture medium was reduced from 20% to 10%, and cells were grown in regular 100 mm tissue culture dishes (BD Biosciences).

A mesenchymal progenitor identity was confirmed in representative colonies by fluorescence-activated cell sorting analysis. Briefly, cells were detached with a dissociation reagent (Sigma-Aldrich, St Louis, MO) for 15 minutes, washed in phosphate-buffered saline (PBS), and incubated for 30 minutes with unconjugated, mouse monoclonal antibodies

previously validated for use in rabbits, namely for CD44 (Antigenix, Huntington Station, NY); CD45 (Antigenix); and CD90 (BD Biosciences). After several washes in 0.1% bovine serum albumin (Sigma-Aldrich), the cells were put on ice for an additional 20 minutes with a fluorescein isothiocyanate (FITC)-conjugated goat anti-mouse immunoglobulin (1:100 dilution, STAR9B, AbD Serotec, Raleigh, NC). Nonspecific cell staining was excluded using a mouse isotype immunoglobulin control. Between 5,000 and 10,000 labeled cells were acquired and analyzed using the Vantage SE cell sorter (BD Biosciences).

After 5 to 8 successive passages, cells were labeled with green fluorescent protein (GFP) by retroviral nuclear infection based on methods previously described [10]. Briefly, amphotropic viruses were prepared by cotransfecting the construct pMIG (Addgene, Cambridge MA) with a pCL-10A1 plasmid (Imgenex, San Diego, Calif) into human embryonic kidney 293 cells (Q-Biogene, Montreal, Canada) using the Lipofectamine 2000 transfection reagent (Invitrogen). Supernatants were collected at 48 and 72 hours post-transfection, filtered, and used to infect the aMSCs. Virus-containing medium was removed after a minimum of 12 hours, when fresh culture medium was added. Successful labeling (mean positivity of $42.0 \pm 7.8\%$) was confirmed by flow cytometry using a MoFlo cytometer (Cytomation, Fort Collins, CO).

1.2. Nanofiber Fabrication

Poly-L-lactic acid (PLLA) scaffolds were fabricated according to an electrospinning process previously described [11]. Briefly, 1.6 g of PLLA (Polysciences, Warrington, PA) was dissolved in 10 mL of chloroform for 24 hours at room temperature, after which 1 mL of dimethylformamide was added, followed by 2 hours of vortexing. The resulting 0.145 g/mL polymeric solution was placed in a vertically-fixed 20 mL glass syringe fitted with an 18-G, 10 cm needle. A 16 kV electric field was applied between the needle tip and an aluminum foil sheet covering a rotating copper plate placed 20 cm from the needle tip, leading to a 0.8 kV/cm (voltage/distance) charge density being applied to the polymeric solution as it was sprayed from the needle to the rotating plate. This resulted in PLLA nanofibers of 200–700 nm in diameter being collected onto the plate. The PLLA nanofibrous scaffolds were then sterilized by ultraviolet radiation for 20 min. per side within a laminar flow hood, followed by sequential (100%, 75%, 50%, 25%) ethanol sterilization for 20 min. each, and finally three rinsing cycles in PBS.

1.3. Cell Seeding and 3D Osteogenesis

Scaffold pieces measuring 2×1 cm ($n=6$) were statically seeded with GFP-labelled aMSCs from 6 of the 10 processed amniotic samples, at a density of 40,000 cells/cm². Seeded scaffolds were transferred into 50 mL polypropylene conical tube centrifuge tubes (BD Biosciences) and maintained in an osteogenic medium within a rotating apparatus/bioreactor (Sarstedt AG, Nümbrecht, Germany) at 10 rpm in a 5% CO₂ incubator at 37°C. The osteogenic medium consisted of high-glucose Dulbecco's Modified Eagle Medium (Sigma-Aldrich) supplemented with 5% FBS (Invitrogen), 10,000 U/ml penicillin G sodium (Fisher), 10 mg/mL streptomycin sulfate (Fisher), 5 mM β -glycerophosphate (Sigma), 50 μ M ascorbic acid-2 phosphate (Sigma), and 100 nM dexamethasone (Sigma). Constructs were equally divided into two groups with respect to the time they were left in the bioreactor, namely 14.6 or 33.9 weeks.

Prior to implantation, three-dimensional osteogenesis was assessed in all constructs by both imaging and quantitative extracellular matrix analyses. Imaging was by a Siemens MicroCAT II scanner (Siemens Medical Solutions USA, Hoffman Estates, IL) with 500-micron resolution. Data were acquired with X-ray tube voltage of 60 kVp, currents of 0.500 mA, and 360 steps. A manufacturer supplied phantom provided a linear relationship

between signal intensity and subject density. Construct density was calculated as the mean of 3 axial slices of each specimen using a post-acquisition image analysis freeware (Amide, <http://amide.sourceforge.net>) [12]. Calcium deposition, a surrogate for construct mineralization, was measured spectroscopically by the Calcium Assay Kit (BioAssay Systems, Hayward, CA) according to the manufacturer's instructions. Briefly, the phenosulphonephthalein dye in the kit forms a stable blue colored complex upon binding with free calcium; the absorbency was measured at 605 nm. In like manner, alkaline phosphatase activity, a surrogate for ongoing bone remodeling, was determined spectroscopically by the Alkaline Phosphatase Assay Kit (BioAssay) according to the manufacturer's instructions. Briefly, *p*-Nitrophenol hydrolysis by alkaline phosphatase was determined by measuring the absorbency at 405 nm.

1.4. Engineered Sternal Repair

Weaning kits at 77–78 days old (n=6) were anesthetized with 1–3% isoflurane (Baxter) and received 20mg/kg of Cefazolin (Orchid) intravenously prior to surgical manipulation. Animals underwent a midline thoracotomy and exposure of the sternum. A full thickness partial sternal resection spanning 2–3 intercostal spaces was performed (Figure 1A) without entering any pleural cavity. The sternal defect was then completely closed with an engineered construct, which was sutured to local intercostal muscles, ribs, and residual sternum with simple interrupted 4-0 monofilament polypropylene sutures (Prolene, Ethicon) (Figure 1B,C). The remainder of the chest wall was closed in layers and animals were allowed to recover.

1.5. Engineered Tissue Analysis

Animals were clinically evaluated twice a day by three independent observers. At 2 months post-implantation, all kits underwent a simple chest roentgenogram with both anterior-posterior and lateral views immediately followed by euthanasia and necropsy, when the grafts were inspected *in situ*, then removed *en bloc* for multiple analyses. First, a MicroCT scan of the whole specimen and adjacencies was repeated as detailed above. Construct density was once again calculated as the mean of 3 axial slices of each specimen, with the same phantom and freeware used prior to implantation. Repeat measurements of calcium deposition and alkaline phosphatase activity were performed also as described above. Fresh specimens were viewed under a fluorescent microscope using a GFP-cube (Carl Zeiss); comparable samples from non-manipulated animals served as controls for the presence of auto-fluorescence. For histomorphologic evaluations, specimens were paraffin embedded, sectioned and stained with hematoxylin and eosin, as well as immunohistochemistry for GFP using a monoclonal anti-GFP antibody (JL-8; Clontech, Palo Alto, CA), as detailed elsewhere [13]. Histological examinations were performed under a light microscope (Carl Zeiss) and photographed with a digital camera (Canon Powershot S3 IS, Canon USA, Lake Success, NY).

1.6. Statistical Analysis

Statistical comparisons were by performed by the signed-rank and Wilcoxon tests, using commercially available software (SPSS, Chicago, IL). *P* values of less than 0.05 were considered significant.

2. Results

There were no post-operative complications or mortality after the chest wall reconstructions. Chest roentgenograms performed at 2 months post-implantation showed radio-dense material overlying the repaired defect in all rabbits (Figure 2). Necropsy similarly

demonstrated complete closure of the defect in all animals, with the constructs still distinctly visible amidst native tissue.

2.1. MicroCT Analysis

MicroCT scanning revealed dense fillings within the repaired sternal defect in all animals (Figure 3). Overall, microCT-based construct density measurements increased significantly *in vivo*, going from 1155.48 ± 57.19 mg/cc pre-implantation to 1311.05 ± 53.13 mg/cc at harvest (Wilcoxon $P=0.03$). However, these differences were not statistically significant within each group of grafts with regards to their time in the bioreactor (14.6 or 33.9 weeks).

2.2. Histological Analysis

All implants showed evidence of good engraftment and maintenance of the osteogenic phenotype, displaying typical bone morphology (Figure 4). Despite their allogeneic origin, only very few scattered mononuclear infiltrates were noted in some samples. Evidence of active bone remodeling was frequently found along portions of the periphery of the grafts (Figure 4A). Survival of the donor cells *in vivo* was demonstrated by positive GFP expression in all construct samples (Figure 4C). No GFP-positivity was noted in the sternum away from the repair.

2.3. Extracellular Matrix Analysis

Overall, construct mineralization as determined by comparisons of extracellular calcium levels before (1.91 ± 1.43 OD_{612nm}) and after (1.10 ± 1.31 OD_{612nm}) implantation, did not change significantly *in vivo* (Wilcoxon $P=0.44$). An overall increase in alkaline phosphatase activity pre- (0.68 ± 65.68 UI/L) and post-implantation (255.68 ± 223.86 UI/L) was noted, which bordered on statistical significance (Wilcoxon $P=0.09$). There no statistically significant differences in either of these comparisons within each group of grafts with regards to their time in the bioreactor (14.6 or 33.9 weeks).

3. Discussion

The translational implication of the concept explored herein is self-explanatory. Once the diagnosis of a major congenital chest wall anomaly is made through fetal imaging, an autologous osseous graft would be engineered in parallel to gestation, so that the affected neonate could benefit from its availability immediately after birth. Given the fact that a diagnostic amniocentesis is routinely indicated in the setting of any major congenital structural anomaly, combined with the anticipated autologous use of the engineered bone for chest wall repair, no ethical objections to this therapeutic notion could be justified.

Variations of this therapeutic principle have already been validated experimentally for the repair of congenital diaphragmatic and airway defects [14–16]. The present study further broadens the foreseeable applications of aMSC-based fetal tissue engineering, by including chest wall anomalies in the list of defects amenable to this form of repair. An engineered osseous graft derived from such an easily accessible cell source as the amniotic fluid would offer several advantages over techniques currently available for the repair of severe chest wall anomalies. The engineered approach affords much versatility, as bone grafts can be created into any shape and size, according to the anatomical details of the defect at hand, as determined by fetal imaging. In contrast to the use of heterotopic autologous native tissues, engineered osseous grafts can be made to better mimic the unique structural and biomechanical properties of native bone of a given anatomical site. Donor site morbidity is essentially eliminated with the use of aMSC-based grafts. Finally, the ability to have custom-made osseous tissue may prove particularly useful in cases for which current methods of repair offer little or no hope at all. Indeed, this is why we selected a full

thickness sternal defect for this initial *in vivo* report, so as to be a surrogate for congenital anomalies such as *ectopia cordis*, which, while rare, are often impossible to be closed primarily and continue to be associated with very low survival rates [2].

A successful tissue engineering approach will hinge on the selection of not only a proper cell source, but also suitable scaffolding material. The engineering of extracellular matrix-rich tissue grafts, such as cartilage and bone, normally benefits from an ample framework for cell attachment (surface area-to-volume ratio), which is a pre-requisite for extracellular matrix synthesis, not to mention cell growth and differentiation. A number of scaffolds that would fit that bill have been investigated for bone tissue engineering, notably PLLA-phosphate glass composites [17]; PLLA-hydroxyapatite composites [18]; and PLLA-beta-tricalcium phosphate composites [18]. However, all these scaffolds house microfibers measuring several micrometers in diameter, whereas native collagen fibrils that compose normal extracellular matrices, for example, have diameters ranging from 200 to 700 nanometers. This was the basis for our selection of nanofibers for the present work, as they have a diameter comparable to that of native collagen, hence offering a very high surface area-to-volume ratio. In addition, much like native collagen, nanofibrous scaffolds feature high porosity (90%) and a wide range of pore sizes (5 to 475 μm) [19]. All combined, these characteristics of electrospun nanofibers closely mimic the architectural scale and morphology of natural extracellular matrix [20, 21].

In this introductory, feasibility study, we aimed solely at examining aMSC-based implant engraftment, donor cell survival, and sustained structural repair of a full thickness chest wall defect *in vivo*, all of which could be demonstrated here, along with maintenance of the engineered bone 3D architecture over time. Efficacy studies, for example comparing cell-based constructs with acellular ones, are the next step, now being pursued by our group. The borderline increase in alkaline phosphatase activity noted in this initial series was not statistically significant, likely because of the relatively small number of subjects typical of studies utilizing larger animal models. Yet, combined with the histological findings, these data pointed to continued remodeling of the engineered graft *in vivo*. The overall preservation of construct mineralization after implantation was of note, particularly in light of the heterologous nature of the grafts. Yet, the reasons behind the discrepancy between the lack of difference in calcium levels pre- and post-implantation and the corresponding increase in construct density as measured by microCT are unclear. Protracted maintenance of the grafts in a bioreactor prior to implantation did not have any impact in outcome, or on any of the variables analyzed. This is in accordance with our previously reported *in vitro* data, which have shown that both construct mineralization and remodeling tend to stabilize after 12–16 weeks[6].

We used heterologous, rather than autologous grafts mostly for logistical reasons stemming from the combination of the quite short leporine gestation, the planned very young age of the hosts, and the necessary protracted time for engineered bone fabrication, as the latter demands extensive and time consuming extracellular matrix deposition. In humans, most likely this would not be a hindrance, given the plentiful time between a diagnostic amniocentesis and birth. Still, it is worth noting that there was a paucity of inflammation seen in histology. Perhaps the known immunoregulatory properties of mesenchymal stem cells is also present in aMSCs and may have contributed towards these findings [22–24]. However, this is but speculation at this time.

Certainly, the eventual clinical application of the therapeutic concept described here will demand further experimental development. Autologous models will need to be studied, along with the repair of larger defects and the analysis of longer term outcomes. In addition, the actual engineering of aMSC-based bone can conceivably be enhanced by comparing

numerous different scaffolds and 3D culture conditions. A better understanding of the determining factors for engineered bone remodeling *in vivo*, along with comparisons with other forms of treatment, would also be desirable. At the same time, our recent work on preclinical regulatory validation of aMSC manufacturing should also apply to bone engineering, hence likely expediting its eventual availability to patients [9, 25].

While, not surprisingly, further investigation will be necessary before this principle can be translated into clinical reality, this study suggests that engineered osseous grafts derived from aMSCs can become a practical alternative for perinatal thoracoplasty.

Acknowledgments

The authors thank Dr. Arthur Nedder and Mr. Mark Kelly for their exemplary veterinary care, as well as Ms. Tonora Archibald for her outstanding histology processing.

S.A.S. was supported by the Joshua Ryan Rappaport Fellowship of the Department of Surgery, Children's Hospital Boston.

References

1. Engum SA. Embryology, sternal clefts, ectopia cordis, and Cantrell's pentalogy. *Semin Pediatr Surg.* 2008; 17:154–60. [PubMed: 18582820]
2. Shamberger RC. Congenital chest wall deformities. *Curr Probl Surg.* 1996; 33:469–542. [PubMed: 8641129]
3. Samir K, Ghez O, Metras D, et al. Ectopia cordis, a successful single stage thoracoabdominal repair. *Interact Cardiovasc Thorac Surg.* 2003; 2:611–3. [PubMed: 17670136]
4. Morales JM, Patel SG, Duff JA, et al. Ectopia cordis and other midline defects. *Ann Thorac Surg.* 2000; 70:111–4. [PubMed: 10921692]
5. Alphonso N, Venugopal PS, Deshpande R, et al. Complete thoracic ectopia cordis. *Eur J Cardiothorac Surg.* 2003; 23:426–8. [PubMed: 12614821]
6. Shanti, RM.; Steigman, SA.; Li, WJ., et al. Human fetal bone engineering with electrospun nanofibers and amniotic mesenchymal stem cells. 59th Annual Meeting of the Section on Surgery of the American Academy of Pediatrics; San Francisco, CA. 2007.
7. Kaviani A, Perry TE, Dzakovic A, et al. The amniotic fluid as a source of cells for fetal tissue engineering. *J Pediatr Surg.* 2001; 36:1662–5. [PubMed: 11685697]
8. Kaviani A, Guleserian K, Perry TE, et al. Fetal tissue engineering from amniotic fluid. *J Am Coll Surg.* 2003; 196:592–7. [PubMed: 12691937]
9. Kunisaki SM, Armant M, Kao GS, et al. Tissue engineering from human mesenchymal amniocytes: a prelude to clinical trials. *J Pediatr Surg.* 2007; 42:974–9. discussion 979–80. [PubMed: 17560205]
10. Cherry SR, Biniszkiewicz D, van Parijs L, et al. Retroviral expression in embryonic stem cells and hematopoietic stem cells. *Mol Cell Biol.* 2000; 20:7419–26. [PubMed: 11003639]
11. Li WJ, Cooper JA Jr, Mauck RL, et al. Fabrication and characterization of six electrospun poly(alpha-hydroxy ester)-based fibrous scaffolds for tissue engineering applications. *Acta Biomater.* 2006; 2:377–85. [PubMed: 16765878]
12. Loening AM, Gambhir SS. AMIDE: a free software tool for multimodality medical image analysis. *Mol Imaging.* 2003; 2:131–7. [PubMed: 14649056]
13. Langenau DM, Traver D, Ferrando AA, et al. Myc-induced T cell leukemia in transgenic zebrafish. *Science.* 2003; 299:887–90. [PubMed: 12574629]
14. Fuchs JR, Kaviani A, Oh JT, et al. Diaphragmatic reconstruction with autologous tendon engineered from mesenchymal amniocytes. *J Pediatr Surg.* 2004; 39:834–8. discussion 834–8. [PubMed: 15185207]
15. Kunisaki SM, Fuchs JR, Kaviani A, et al. Diaphragmatic repair through fetal tissue engineering: a comparison between mesenchymal amniocyte- and myoblast-based constructs. *J Pediatr Surg.* 2006; 41:34–9. discussion 34–9. [PubMed: 16410104]

16. Kunisaki SM, Freedman DA, Fauza DO. Fetal tracheal reconstruction with cartilaginous grafts engineered from mesenchymal amniocytes. *J Pediatr Surg.* 2006; 41:675–82. [PubMed: 16567175]
17. Georgiou G, Mathieu L, Pioletti DP, et al. Polylactic acid-phosphate glass composite foams as scaffolds for bone tissue engineering. *J Biomed Mater Res B Appl Biomater.* 2007; 80:322–31. [PubMed: 16838353]
18. Montjovent MO, Mathieu L, Hinz B, et al. Biocompatibility of bioresorbable poly(L-lactic acid) composite scaffolds obtained by supercritical gas foaming with human fetal bone cells. *Tissue Eng.* 2005; 11:1640–9. [PubMed: 16411809]
19. Li WJ, Laurencin CT, Catterson EJ, et al. Electrospun nanofibrous structure: a novel scaffold for tissue engineering. *J Biomed Mater Res.* 2002; 60:613–21. [PubMed: 11948520]
20. Christenson EM, Anseth KS, van den Beucken JJ, et al. Nanobiomaterial applications in orthopedics. *J Orthop Res.* 2007; 25:11–22. [PubMed: 17048259]
21. Barnes CP, Sell SA, Boland ED, et al. Nanofiber technology: designing the next generation of tissue engineering scaffolds. *Adv Drug Deliv Rev.* 2007; 59:1413–33. [PubMed: 17916396]
22. Arinze TL, Peter SJ, Archambault MP, et al. Allogeneic mesenchymal stem cells regenerate bone in a critical-sized canine segmental defect. *J Bone Joint Surg Am.* 2003; 85-A:1927–35. [PubMed: 14563800]
23. Gotherstrom C, Ringden O, Tammik C, et al. Immunologic properties of human fetal mesenchymal stem cells. *Am J Obstet Gynecol.* 2004; 190:239–45. [PubMed: 14749666]
24. Barry FP, Murphy JM, English K, et al. Immunogenicity of adult mesenchymal stem cells: lessons from the fetal allograft. *Stem Cells Dev.* 2005; 14:252–65. [PubMed: 15969620]
25. Steigman SA, Armant M, Bayer-Zwirello L, et al. Preclinical regulatory validation of a 3-stage amniotic mesenchymal stem cell manufacturing protocol. *J Pediatr Surg.* 2008; 43:1164–9. [PubMed: 18558201]

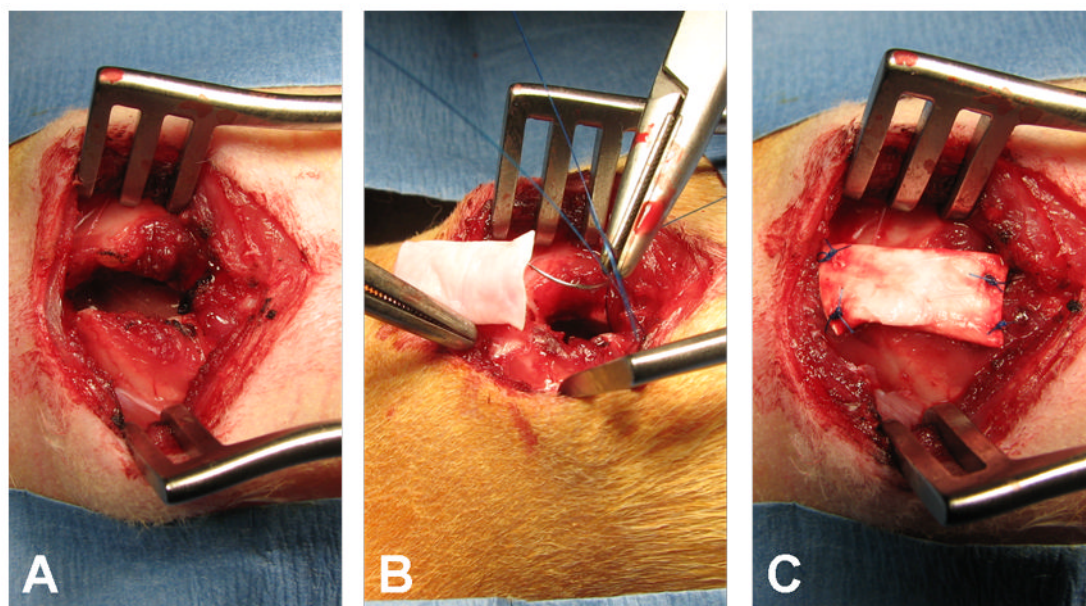


Figure 1. Sequence of repair of a surgically created full thickness sternal defect with an engineered osseous graft, in a rabbit kit. Representative intraoperative photographs of (A) the sternal defect; (B) the graft being sewn into place; and (C) the repair of the defect nearing completion.

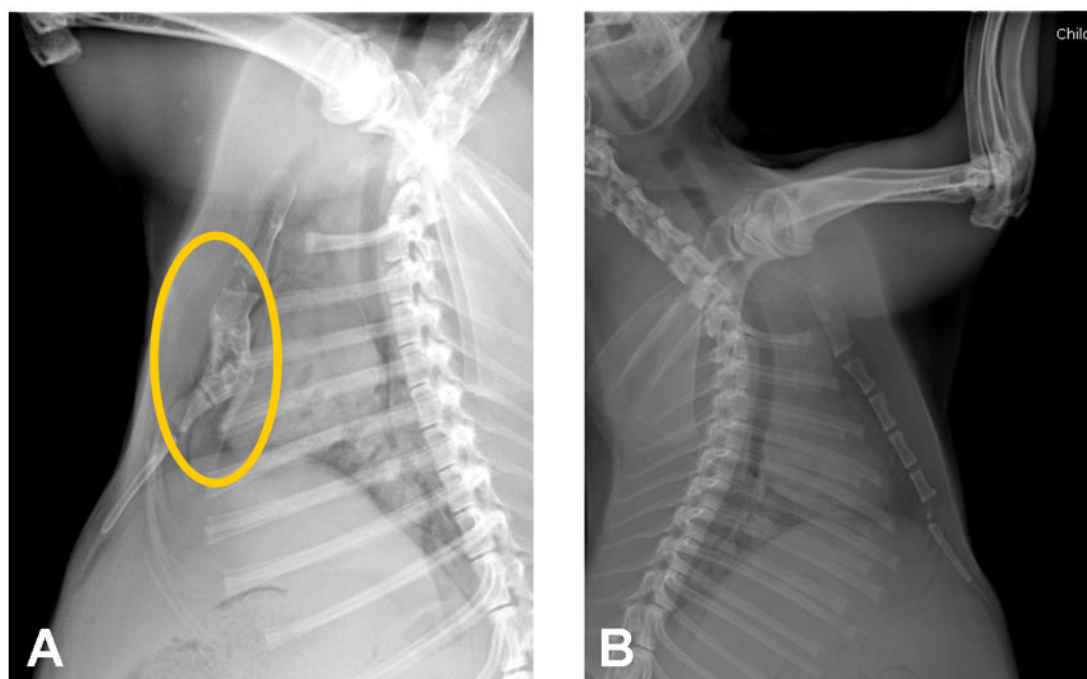


Figure 2. (A) Lateral view of a chest roentgenogram performed 2 months after implantation of an engineered osseous graft in the sternum (within the ellipse), in a rabbit kit. (B) A comparable image from an age-matched normal animal.

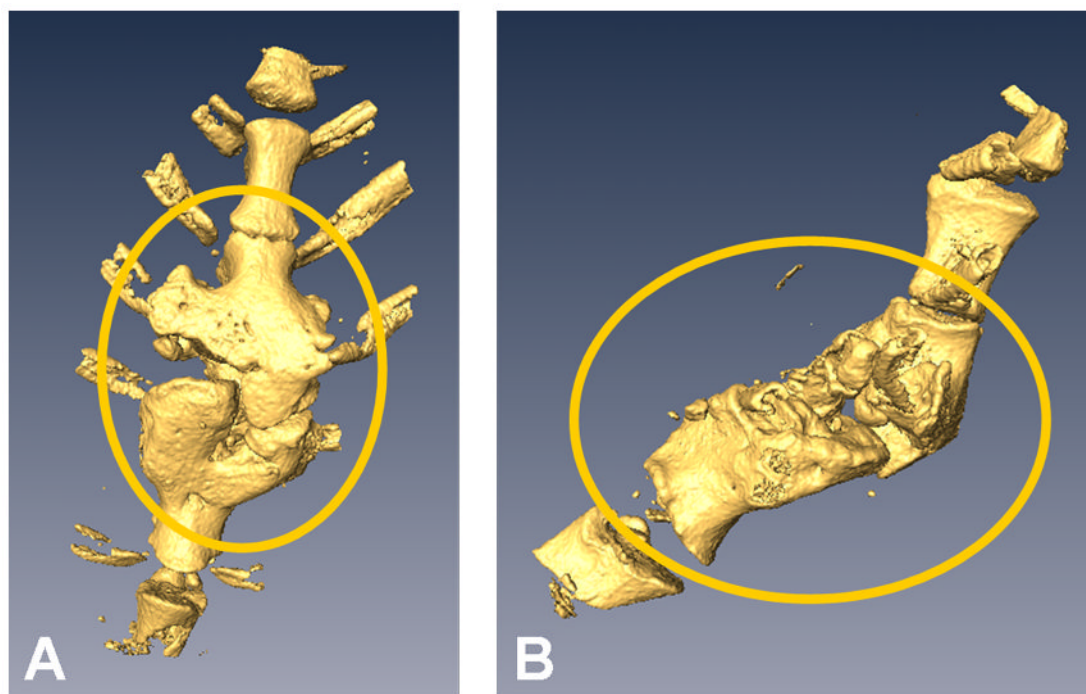


Figure 3. Representative three-dimensional microCT scan of the sternum performed 2 months after local implantation of an engineered osseous graft (within the ellipses), in a rabbit kit: (A) coronal view; (B) sagittal view.

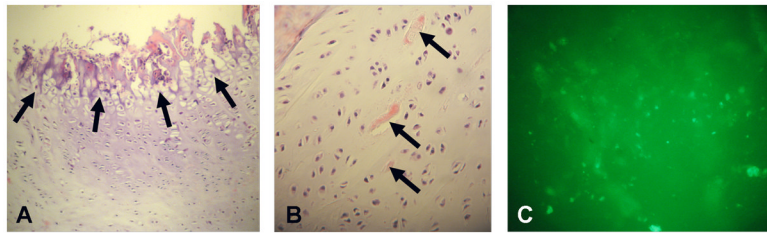


Figure 4.

Representative photomicrographs of engineered osseous grafts *in vivo*. (A) The arrows point to an area of active bone remodeling in the periphery of the graft, as evidenced by the typical increased vacuolization of the cell-harboring lacunae (magnification, x100). (B) The arrows point to nanofiber remnants within the graft (magnification, x200). (C) Positive green fluorescent protein expression (bright spots) under dissection fluorescence microscopy of a fresh specimen, indicating survival of the donor cells *in vivo* (magnification, x100).